Mechanics of Time-Dependent Materials (2026) 30:5
https://doi.org/10.1007/s11043-025-09849-x

RESEARCH

Dual modeling of unsteady radiative non-Newtonian fluid flow with Biot boundary conditions using novel time-dependent solutions

S.M. Sachhin[1] · M.S. Bharath[1] · U.S. Mahabaleshwar[1] · G.V. Bognar[2] · L.M. Pérez[3]

Received: 26 September 2025 / Accepted: 19 December 2025

Abstract
This analysis gives insight into unsteady radiative energy and Casson fluid flow across stretching and shrinking sheets with Biot boundary conditions, enhancing our comprehension of these intricate conditions. Examined the two mathematical representations with the help of a rigorous method. The initial model aligns with the approach usually used by researchers in this area, but its stationary solution stays trivial. The second method clearly illustrates the physically pertinent stationary solutions well examined in published works. In particular, unveiled the new similarity variables specifically for the energy equation solely within the initial model. Utilized the numerical method to solve the governing partial differential equations, while similarity variables can describe particular scenarios with uniform wall temperatures, more general cases may require non-similar analysis to fully capture heat transfer variations. Here, both analytical hypergeometric series and numerical methods were employed to study the impact of various physical impacts on boundary layer flows. The results of the current analysis reveal that enhance in thermal radiation and Biot number enhances the surface heat transfer by nearly 30%, while wall suction further improves it by about 22%. Similarly, a stretching boundary contributes an additional 18% rise compared to the shrinking case. Moreover, analyzing several non-Newtonian fluids provided insight into implications for related stagnation points and viscoelastic problems. A diversity of analytical approaches and computational techniques can thereby elucidate subtleties in transport for diverse geometries and material behaviours.

Keywords Unsteady flow · Thermal radiation · Casson fluid · Analytical and numerical method · Biot number

Nomenclature

List of symbols

Cp	Specific heat co-efficient
d	Stretching/shrinking parameter
$f(\eta)$	Velocity function
Nr	Radiation
Pr	Prandtl number
P	Pressure

Extended author information available on the last page of the article

Published online: 05 January 2026

q_r	Radiative heat flux
S	Mass suction/injection parameter
t	Time
T_w	Surface Temperature
T	Fluid Temperature
T_∞	Ambient temperature
u, v	velocities
u_w	Velocity
v_w	Wall velocity
x, y	Coordinates

Greek symbols

$A(\tau), B(\tau), \sigma(\tau)$	Constants
λ	Solution value
η	Similarity variable
Λ	Casson parameter
k^*	Absorption coefficient
ψ	Stream function
σ^*	Stephen Boltzmann constant
$\theta(\eta)$	Dimension less temperature

Abbreviation

B. Cs	Boundary conditions
MHD	Magnetohydrodynamics
hnf	Hybrid nanofluid
nf	Nanofluid
tnf	Ternary nanofluid
ODE	Ordinary Differential Equation
PDE	Partial Differential Equation

1 Introduction

In modern days, Casson fluids applications have gained the attention of many researchers. Casson fluid, characterized by its yield stress and plastic viscosity, is a non-Newtonian fluid that has found significant applications in various industries due to its unique flow properties. It is particularly relevant in the field of biomechanics, where it serves as an ideal model for blood flow in cardiovascular research, aiding in the design of medical devices such as blood oxygenators and hemodialyzers. In the polymer industry, Casson fluid dynamics are crucial for understanding and controlling the behavior of materials during processing. The Casson model also plays a vital role in the food and pharmaceutical sectors, where precise flow control is necessary to ensure product quality and safety. Moreover, in the realm of energy engineering, Casson fluid flow analysis contributes to the optimization of thermal management systems, increasing the efficiency of thermodynamic systems. Arthur et al. (2015) studied the Casson fluid movement across a vertical permeable surface with a chemical reaction with a magnetic field. Animasaun et al. (2016) examined the motion of energy-dependent steady incompressible free convective Casson fluid flow over an exponential surface. Shah et al. (2022) studied the effect of convective energy transport on Casson fluid on curved cavity with MHD. Mittal and Patel (2020) studied the 2-D mixed convective flow of Casson fluid across an infinite sheet. Mahabaleshwar et al. (2024) studied the viscosity ratio effect in non-Newtonian fluids with various boundaries.

Thermal radiation significantly impacts fluid flow in various engineering and environmental processes. It is a form of heat transfer where energy is emitted by a surface at a finite temperature and can affect the temperature distribution within a fluid, altering its viscosity and flow characteristics. In industrial applications, understanding thermal radiation can optimize processes like cooling systems in nuclear reactors, where heat removal is crucial for safety and efficiency. In natural settings, thermal radiation influences weather patterns and ocean currents by affecting the temperature gradients in the atmosphere and bodies of water. The study of thermal radiation in fluid flow is vital for the development of efficient energy systems, enhancing environmental modeling, and improving climate prediction accuracy. By mastering this knowledge, engineers and scientists can design better equipment and predict natural phenomena with greater precision, leading to advancements in technology and a deeper understanding of our world. Yu and Wang (2022) explored the energy and fluid flow movement across two expanding rotating disks with carbon nanotubes. Lorentz force impact on ferro fluid movement has been explored by Sachhin et al. (2025d). Sheremet and Pop (2018) studied the convective heat transfer in fluid flow via heated square cavity. Energy transfer effects on the movement of fluid through expanding surfaces studied by Hashim et al. (2018a), Sachhin et al. (2025a).

The study of fluid flow across stretching sheets is pivotal in various industrial processes due to the unique characteristics it imparts to the fluid dynamics. For instance, in the field of aerodynamics, the stretching of surfaces affects the boundary layer control, which is crucial for reducing drag on aircraft surfaces. In the manufacturing sector, the extrusion of plastic sheets and metal cooling processes are heavily reliant on the principles of fluid flow over stretching surfaces. This phenomenon is also essential in the polymer industry. Moreover, the stretching surface concept is applied in biotechnology to microfluidic devices that manipulate small fluid volumes, which are essential for various assays and diagnostics. The importance of this study is further underscored by its applications in heat exchangers and crystal growth technologies, where the precise control of fluid flow is necessary for optimal performance and quality. Thus, understanding the fluid flow over stretching surfaces not only enhances the efficiency of industrial processes but also contributes to advancements in technology and materials science. The viscous fluid generated by a contrasting sheet was examined by Sakiadis (1961), who found both numerical and in-closed form solutions. The energy transfer and movement of a non-Newtonian liquid past an expanding sheet have been studied by Crane (1970). Unsteady viscous fluid movement across a curved surface has been studied by Roşca and Pop (2015). Unsteady fluid flow of a power-law nanofluid across an expanding surface has been studied by Khalili et al. (2015), Nandy (2015). Miklavčič and Wang (2006) studied the viscous fluid flow past contrasting surfaces.

The Biot number, a dimensionless parameter named after the French physicist Jean-Baptiste Biot, which is instrumental in predicting temperature distribution within a solid object exposed to a fluid flow. For instance, in systems with a Biot number much less than one, the internal temperature of the object can be assumed to be uniform, simplifying the analysis of heat transfer significantly. Conversely, a Biot number greater than one indicates a non-uniform temperature within the object, necessitating a more complex approach to account for internal thermal gradients. This distinction is vital for engineers and scientists when designing and optimizing equipment such as heat exchangers, where accurate control of temperature profiles is essential for efficiency and safety. Moreover, the Biot number's significance extends to various industries, including aerospace, automotive, and manufacturing, where understanding the interplay between conductive and convective heat transfer can lead to innovations in material science and thermal management systems. Prasad et al. (2014) examined the nonlinear steady Eyring fluid with heat transfer across a vertical sheet. Bég et al. (2014) explored the heat transfer by magneto-convective movement of fluid flow inside a radiating vertical surface. Cooling effective pin structures have been experimentally studied by Liu et al. (2021) in the wind tunnel. Magnetic fluid movement with energy transfer across external surfaces has been studied by Amanulla et al. (2018), Gaffar et al. (2015), Sachhin et al. (2025b), Turkyilmazoglu (2024), Sachhin and Mahabaleshwar (2025).

Kumar et al. (2025) studied the Casson term influence on convective fluid flow inside vertical permeable plates using a finite difference method. Mohamad Isa et al. (2025) examined the Lorentz force influence on dusty fluid flow on vertical expanding sheet.Srinivas et al. (2024) examined the effect of velocity slip on fluid movement by using a Galerkin finite element approach. Goud et al. (2024) studied the influence of heat source on nanofluid movement inside porous media with mass transfer. Gosty et al. (2024) conducted research on variable viscosity impact on micropolar fluid. Dharmaiah et al. (2024), Sachhin et al. (2025c), Bataller (2007) conducted research on the Lorentz force on fluid movements through various surfaces. The Galerkin finite element technique utilized by Kazmi et al. (2024) to explore the hybrid nanofluid movement across a square lid. Hussain et al. (2024a) analysed the thermophoresis impact on Carreau nano-Newtonian fluid movement across expanding surfaces. Awais et al. (2017) analysed the mixed convection impact on Sisko fluid movement through linearly expanding cylinders. Hussain and Malik (2021), Hussain et al. (2024b), Hayat et al. (2011), Ibrahim and Shankar (2013) examined the Lorentz force influence nanofluid movements.

Hashim et al. (2019) explored the energy transfer impact Williamson fluid flow, Hamid et al. (2019) examined the stability and solar radiation influence on nanofluid movement, Hashim et al. (2018b) studied the nanoparticle and stability analysis influence on transient Carreau fluid flow using critical points, Basir et al. (2020) explored the bioconvection impact on moving surface. Saif et al. (2021) examined the slip and energy transfer impact on thermally stratified fluid. Darvesh et al. (2024a), Aljedani et al. (2024), Darvesh et al. (2025) analysed the Lorentz force effect on fluid movement. Deepalakshmi et al. (2025) examined the solar radiation influence on Casson fluid movement via renal tubes. Darvesh et al. (2024b) explored the heat transfer influence on Cross fluid movement using numerical approach. Razzaq et al. (2023), Razzaq and Farooq (2025) explored the nano fluid movement via elastic surface. Farooq et al. (2021) studied the viscosity influence on convective fluid movement across expanding sheet. Razzaq et al. (2024) explored the Lorentz force influence on Casson fluid movement across inclined sheet. Sagheer et al. (2024), Hussain et al. (2023) analysed the radiation influence on fluid boundary layer.

1.1 Motivation and novelty

Based on the above references, we have shown conclusively that the unsteady flow equations considered do not become steady-state in their long-time limit as is expected for real flow phenomena. In fact, with very few exceptions, all of these types of equations quickly decay and settle down into the unsteady flow state that was assumed to describe fluid flow before motion ever started. The novelty of the current analysis lies in the study of unsteady radiative heat transfer and Casson fluid flow analysis with novel time-dependent solutions under Biot boundary conditions using both analytical and numerical methods. However, the Sakiadis (1961), Crane (1970), and Miklavčič and Wang (2006) models constitute state solutions for the full Navier-Stokes equations, but their unsteady flow has not been explored, which is a notable research gap. The absence of any analysis along these lines prompted us to give a thorough look at unsteady Navier-Stokes equations and work out models for the trivial solution and also for Sakiadis (1961), Crane (1970), Miklavčič and Wang (2006), and nonzero physical solutions as steady states. Furthermore, the corresponding unsteady energy equation as well as new time-dependent temperature solutions are discussed here. A few things are notable from the temperature results. First, only when a shrinking sheet is used is this improved heat transfer possible. The present analysis will without a doubt be very useful to researchers doing unsteady flow and heat transfer problems on strip and truckle sheets.

1.2 Research questions can be addressed by the current study

i. How can the unsteady Navier-Stokes equations be reformulated to generate nontrivial long-time solutions that converge to the classical Sakiadis-Crane and Miklavčič-Wang steady states, unlike the models commonly used in previous studies?
ii. What mathematical formulations lead to the emergence of two distinct unsteady flow models, and how do these conditions impact the physical characteristics of expanding and shrinking boundary-layer flows?
iii. In what ways do the newly developed similarity transformations for the temperature field modify the predicted energy-transfer characteristics, and under what circumstances do they reveal optimal energy performance at uniform wall temperature?
iv. How do key physical parameters such as the Casson parameter, stretching term, radiation effect, Biot number, and mass suction/injection affect the momentum and energy fields within the proposed unsteady models, and what applications do these effects have for practical energy-transfer applications?

2 Mathematical model

Considered incompressible, laminar, Casson fluid, A sufficiently long one-dimensional sheet is assumed to deform via either a prescribed stretching or shrinking process to induce a two-dimensional flow field just above the wall as configured in Fig. 1(a).

2.1 Assumptions and restrictions of the current analysis are as follows

- Considered non-Newtonian fluid because of its fluid viscosity being dependent on the shear rate.
- Studied laminar, incompressible, non-Newtonian flow.
- Considered a stretching/shrinking surface.
- Assumed unsteady steady incompressible flow.
- Assuming surface velocity $u\,(x, y = 0, t) = aA\,(t)\,x$.

The rheological equation of Casson fluid the given as follows (Sachhin et al. 2025b; Turkyilmazoglu 2024; Sachhin and Mahabaleshwar 2025).

$$\tau_{ij} = \begin{cases} 2(\mu_B + p_y/\sqrt{2\pi})e_{ij}, & \pi > \pi_c, \\ 2(\mu_B + p_y/\sqrt{2\pi_c})e_{ij}, & \pi < \pi_c, \end{cases} \tag{1}$$

the yield stress P_y is considered as $P_y = \frac{\mu_B\sqrt{2\pi_c}}{\Lambda}$, π and π_c are deformation rate product and product value, P_y and μ_B are yields stress and viscosity of plastic deformation. The unsteady Casson-fluid flow phenomenon is due to the continuity and Navier–Stokes equations

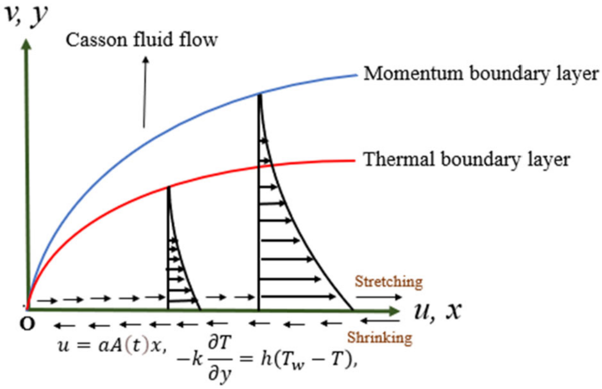

(a)

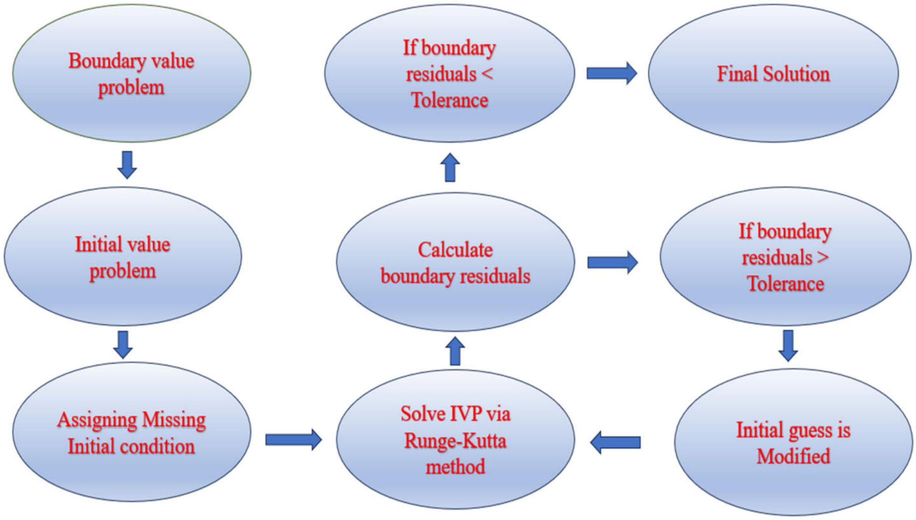

(b)

Fig. 1 (a): Schematic diagram. (b): Flow chart of numerical approach

(Sachhin et al. 2025b; Turkyilmazoglu 2024; Sachhin and Mahabaleshwar 2025):

$$\frac{\partial u}{\partial x} + \frac{\partial v}{\partial y} = 0, \tag{2}$$

$$\frac{\partial u}{\partial t} + u\frac{\partial u}{\partial x} + v\frac{\partial u}{\partial y} = -\frac{1}{\rho}\frac{\partial p}{\partial x} + \frac{\mu}{\rho}\left(1 + \Lambda^{-1}\right)\left(\frac{\partial^2 u}{\partial x^2} + \frac{\partial^2 u}{\partial y^2}\right), \tag{3}$$

$$\frac{\partial v}{\partial t} + u\frac{\partial v}{\partial x} + v\frac{\partial v}{\partial y} = -\frac{1}{\rho}\frac{\partial p}{\partial y} + \frac{\mu}{\rho}\left(1 + \Lambda^{-1}\right)\left(\frac{\partial^2 v}{\partial x^2} + \frac{\partial^2 v}{\partial y^2}\right), \tag{4}$$

$$\frac{\partial T}{\partial t} + u\frac{\partial T}{\partial x} + v\frac{\partial T}{\partial y} = \frac{\kappa}{\rho Cp}\frac{\partial^2 T}{\partial y^2} - \frac{1}{\rho Cp}\frac{\partial q_r}{\partial y}. \tag{5}$$

Complemented boundary and initial conditions (Sachhin et al. 2025b; Turkyilmazoglu 2024):

$$u\left(x, y=0, t\right)=aA\left(t\right)x, \tag{6(a)}$$

$$v\left(x, y=0, t\right)=V_w\left(t\right), \tag{6(b)}$$

$$u\left(x, y\to\infty, t\right)=0, \tag{6(c)}$$

$$u\left(x, y, t=0\right)=u_0\left(x, y\right), \tag{6(d)}$$

$$-\kappa\frac{\partial T}{\partial y}\left(x, y=0, t\right)=h\left(T_w-T\right), \tag{6(e)}$$

$$T\left(x, y\to\infty, t\right)=T_\infty, \tag{6(f)}$$

$$T\left(x, y, t=0\right)=T_0\left(x, y\right), \tag{6(g)}$$

here u and v are the momentum terms components along x and y axis, p is the pressure, Λ is Casson parameter, ρ is density, κ is thermal conductivity, Cp heat capacitance.

The Rosseland's method for formulating heat flux radiation q_r as follows (Sachhin et al. 2025b; Sachhin and Mahabaleshwar 2025).

$$q_r=-\frac{4\sigma^*}{3k^*}\frac{\partial T^4}{\partial y}. \tag{7}$$

To expand T^4 with Taylor series method, and eliminate the upper order terms obtains:

$$T^4\cong 4T_\infty^3T-3T_\infty^4, \tag{8}$$

the radiation term in Eq. (5) is differentiated and produced in the form of

$$\frac{\partial q_r}{\partial y}=-\frac{16\sigma^*T_\infty^3}{3k^*}\frac{\partial^2 T}{\partial y^2}. \tag{9}$$

Adding Eq. (9) and Eq. (5) we get

$$\frac{\partial T}{\partial t}+u\frac{\partial T}{\partial x}+v\frac{\partial T}{\partial y}=\left(\frac{\kappa}{\rho Cp}+\frac{1}{\rho Cp}\frac{16\sigma^*T_\infty^3}{3k^*}\right)\frac{\partial^2 T}{\partial y^2}. \tag{10}$$

Regarding the above physical flow described by the system Eq. (2)–(5), the following remarks should be given close attention.

- The flow is induced by the horizontal action of the wall due to Eq. (6(a)) and it is absorbed/fed by virtue of the wall transpiration Eq. (6(b)). Under ideal circumstances, whenever (Sachhin et al. 2025b; Turkyilmazoglu 2024).

$$\lim_{t\to\infty}A\left(t\right)=1, \tag{11}$$

$$\lim_{t\to\infty}V_w\left(t\right)=\text{constant}=v_w, \tag{12}$$

then the nonvanishing Sakiadis-Crane solutions (Sakiadis 1961; Crane 1970) should be attained for $a>0$ (stretching sheet); otherwise, the Miklavcic and Wang solutions (Miklavčič and Wang 2006) should be reached for $a<0$ (shrinking sheet). In fact, conditions (11) and

(12) are necessary for the flow field to reach and evolve into the non-trivial steady-state, see the Model 2 below. Otherwise, trivial steady-state can be attained only as shown later in Model 1.

- The far-field condition (6(c)) implies that, on the one hand, the free streamwise flow is not permitted so that the effect of the wall deformation dies out in the streamwise direction far away from the surface. On the other hand, there is no such a restriction on the form of the axial flow, except the mass conservation Eq. (2) dictates that

$$\lim_{y\to\infty} v = \text{constant}. \tag{13}$$

- Application of the far field condition (6(c)) together with Eq. (13) implies that $\frac{\partial p}{\partial x} \to 0$ from Eq. (3); hence, Eq. (3) should be replaced with

$$\frac{\partial u}{\partial t} + u\frac{\partial u}{\partial x} + v\frac{\partial u}{\partial y} = \frac{\mu}{\rho}\left(1+\Lambda^{-1}\right)\left(\frac{\partial^2 u}{\partial x^2} + \frac{\partial^2 u}{\partial y^2}\right), \tag{14}$$

so, Eq. (2) and (14) are adequate for determination of the flow field (u, v). Additionally, Eq. (4) can be made use of finding the deforming pressure gradient $\frac{\partial p}{\partial y}$, and hence $p\ (y, t)$. Now, let us consider the variables and similarity transformations (Sachhin et al. 2025b; Turkyilmazoglu 2024; Sachhin and Mahabaleshwar 2025):

$$\begin{aligned} &\tau = at, \qquad \eta = \sqrt{\frac{a}{\nu}}\sigma(\tau)\, y, \qquad \eta_\tau = \frac{\dot\sigma(\tau)}{\sigma(\tau)}\eta, \\ &u = aA(\tau)\, x f'(\eta), \qquad v = -\sqrt{a\nu}B(\tau)\, f(\eta), \end{aligned} \tag{15}$$

which means that we force the flow field to entail separable solutions in terms of variables (x, η, τ). The motivation behind the above similarity variables and transformations is to discover novel solutions and also to recover the limiting steady/unsteady flow solutions frequently studied in the literature. Additionally, Eq. (15) shapes out the initial velocity in Eq. (6(d)) in the form

$$u_0(x, y) = aA(0)\, x f'(\eta)\big|_{\tau=0}, \tag{16}$$

on substitution of Eq. (15) in Eq. (2), it is found that

$$\sigma(\tau) = \frac{A(\tau)}{B(\tau)}, \tag{17}$$

again, by neglecting pressure term and substituting Eq. (15) into Eq. (14), it reduces to

$$\left(1-\Lambda^{-1}\right) f'''(\eta) + \frac{A}{\sigma^2}\left(f(\eta) f''(\eta) - f'(\eta)^2\right) - \frac{\dot A(\tau)}{A\sigma^2} f' - \frac{\dot\sigma(\tau)}{\sigma^3}\eta f''(\eta) = 0. \tag{18}$$

Model 1 *In order to achieve similarity equation from Eq.* (18), *one of the possibilities is that the coefficients*

$$\frac{A(\tau)}{\sigma(\tau)^2}, \qquad \frac{\dot A(\tau)}{A(\tau)\sigma(\tau)^2}, \qquad \frac{\dot\sigma(\tau)}{\sigma(\tau)^3},$$

must be all constants. This consequently results in

$$\sigma = B = \sqrt{A},$$

as a result of Eq. (18). *This will later imply from Eq.* (17) *that*

$$\frac{\dot{A}}{A^2} = \text{constant} = \alpha,$$

yielding

$$A = \frac{1}{1 - \alpha\tau}, \tag{19}$$

where $\alpha < 0$ (*strictly for the physical possibility of the solutions, otherwise finite time blow-up takes place*) *is called the unsteadiness parameter. Moreover, again from Eq.* (18), *we have*

$$\frac{\dot{\sigma}}{\sigma^3} = \frac{\alpha}{2},$$

which enables us to convert Eq. (18) *into similarity ordinary differential equations*

$$\begin{aligned} &\left(1 + \Lambda^{-1}\right) f''' + ff'' - f'^2 - \alpha\left(f' + \frac{\eta}{2} f''\right) = 0, \\ &f(0) = S, \qquad f'(0) = d, \qquad f'(\infty) = 0. \end{aligned} \tag{20}$$

System of Eq. (20) *admits exponential solutions* (*Sachhin et al.* 2025*b*; *Turkyilmazoglu* 2024; *Sachhin and Mahabaleshwar* 2025):

$$f = S + \frac{d}{\lambda}\left(1 - e^{-\lambda\eta}\right), \tag{20a}$$

by using above equation, Eq. (20) *solved as*

$$2\left(1 + \Lambda^{-1}\right)\lambda^2 - (2S\lambda + \alpha\eta)\lambda - 2d - \alpha = 0, \tag{20b}$$

above binary equations having roots

$$\lambda = \frac{2S + \alpha\eta \pm \sqrt{(-2S - \alpha\eta)^2 - 8(-2d - \alpha)\left(1 + \frac{1}{\Lambda}\right)}}{4\left(1 + \frac{1}{\Lambda}\right)}, \tag{20c}$$

it is noted that in Eq. (20), $d = \pm 1$ *represents the stretching and shrinking scenarios, respectively. Even though the presented model in Eq.* (20) *is similar to the studied ones in the literature, it is somewhat different from them due to the second boundary condition, which is constant here since the literature uses a parameter in place of that. Also, the parameter S in Eq.* (20).

$$\begin{aligned} &u = a\frac{1}{1 - a\alpha t} x f'(\eta), \quad v = -\sqrt{a\nu}\frac{1}{\sqrt{1 - a\alpha t}} f(\eta), \\ &\eta = \sqrt{\frac{a}{\nu}}\frac{1}{\sqrt{1 - a\alpha t}} y, \\ &\frac{p}{\rho} = p_\infty - a\nu\left[Af' + \frac{A^2}{2} f^2 - \lambda^2\left(A - A^2\right)\int f\, d\eta\right]. \end{aligned} \tag{21}$$

Theorem 1 *The unsteady system Eqs. (2)–(6(d)) with the initial condition Eq. (16) has the steady-state trivial solutions on the condition that the time-dependent term $A(\tau)$ is expressed by Eq. (19). The leading velocity and temperature field are given by Eq. (21).*

Proof Closely pursuing the steps in this section through Eqs. (19)–(21) completes the proof. It is time to emphasize that the above unsteady flow model in Eq. (21) is based on the most frequently studied equations in the literature (see the cited references, with only slightly different modifications due to extra physical features), but it does not evolve into the Sakiadis (1961), Crane (1970) as well as Miklavčič and Wang (2006) physical nontrivial steady-state solution in the long-time span. □

Model 2 *In order to be consistent with the Sakiadis (1961), Crane (1970) as well as the Miklavčič and Wang (2006) physical solution, the limiting condition $\alpha = 0$ in Eq. (11) must strictly hold, which is possible only when in Eq. (19), which is itself the steady-state solution. Otherwise, for a finite the system Eq. (20) does not match with the Sakiadis (1961), Crane (1970) as well as the Miklavčič and Wang (2006) physical solution, but it only represents an unsteady solution damping toward the equilibrium solution of zero for large time. Actually, the hint for Eq. (18) to be in line with the Sakiadis (1961), Crane (1970) as well as Miklavčič and Wang (2006) physical solution lies within the term*

$$\frac{\dot{\sigma}}{\sigma^3}, \textit{ multiplying } \eta \textit{ that must vanish, requiring that } \sigma = \text{constant} = 1.$$

Without the loss of generality. So, in this case from Eq. (17), we have $B(\tau) = A(\tau)$. In the light of these, Eq. (18) can be rewritten as

$$\begin{gathered}\left(1-\Lambda^{-1}\right) f''' + A\left(ff'' - f'^2\right) - \frac{\dot{A}}{A} f' = 0, \\ f(0) = S, \quad f'(0) = d, \quad f'(\infty) = 0.\end{gathered} \tag{22}$$

Where the parameter S now is given by

$$S = -\frac{V_w(t)}{\sqrt{a\nu}A} = -\frac{A v_w}{\sqrt{a\nu}A} = -\frac{v_w}{\sqrt{a\nu}},$$

on the other hand, system, Eq. (22) admits exponential type solution

$$f = S + \frac{d}{\lambda}\left(1 - e^{-\lambda\eta}\right), \tag{23}$$

in which $\lambda > 0$ is an eigenvalue to be determined. Substituting Eq. (23) into Eq. (21) gives rise to the relation

$$\dot{A} + (d + S\lambda) A^2 = \lambda^2 A \left(1 - \Lambda^{-1}\right), \tag{24}$$

that determines the amplitude function $A(\tau)$. Prior to that, because of the fact exhibited by Eq. (11) as $\tau \to \infty$, Eq. (24) imposes an eigen relation for λ expressed by

$$d + S\lambda = \lambda^2 \left(1 - \Lambda^{-1}\right), \tag{25}$$

thus, from Eqs. (23) and (24), we reach an ordinary differential equation

$$\dot{A} + \lambda^2 \left(1 - \Lambda^{-1}\right)\left(A^2 - A\right) = 0,$$

generating the amplitude solution by using $\Lambda \to \infty$,

$$A = \frac{e^{\lambda^2 \tau}}{u_a + e^{\lambda^2 \tau}}, \tag{26}$$

with $u_a > 0$ (*strictly for the physical possibility of the solutions otherwise finite time blow-up takes place*) *is the unsteadiness parameter for the present new model. As a result, from Eqs*. (15), (23), *and* (26), *we have the velocity and pressure fields*

$$\begin{aligned} & u = a\frac{e^{\lambda^2 at}}{u_a + e^{\lambda^2 at}} x f'(\eta), \quad v = -\sqrt{a\nu}\frac{e^{\lambda^2 at}}{u_a + e^{\lambda^2 at}} f(\eta), \\ & \eta = \sqrt{\frac{a}{\nu}} y, \\ & \frac{p}{\rho} = p_\infty - a\nu\left[Af' + \frac{A^2}{2} f^2 - \lambda^2\left(A - A^2\right)\int f d\eta\right]. \end{aligned} \tag{27}$$

Theorem 2 *The unsteady system Eqs*. (2) *to* (6(*d*)) *with the initial condition* (16) *has the steady-state Sakiadis* (1961), *Crane* (1970) *or Miklavčič and Wang* (2006) *physical solutions provided that the time-dependent term* $A(\tau)$ *is expressed by Eq*. (26). *The leading velocity and temperature field are given by Eq*. (27).

Proof Following the previous steps from Eqs. (22)–(27) will complete the proof. □

Corollary 1 *In view of the form of the solutions in Eqs*. (22) *and* (27), *the wall shear of engineering interest in Models* 1 *and* 2 *is given, respectively, by means of*

$$\begin{aligned} & \left.\frac{\partial u}{\partial y}\right|_{y=0} = a\sqrt{\frac{a}{\nu}}\frac{1}{\sqrt{(1-a\alpha t)^3}} x f''(0), \\ & \left.\frac{\partial u}{\partial y}\right|_{y=0} = a\sqrt{\frac{a}{\nu}}\frac{e^{\lambda^2 at}}{u_a + e^{\lambda^2 at}} x f''(0). \end{aligned} \tag{28}$$

3 Analysis of the temperature field

Energy equation is Eq. (5) and (6(e))–(6(g)) gives the boundary conditions, with the transformations in Eq. (15) as well as the separable temperature field

$$T = T_\infty + T_a T_w(\tau)\left(\frac{x}{l}\right)^n \theta(\eta). \tag{29}$$

Equations (5) and (6(e))–(6(g)) are converted to

$$\begin{aligned} & \frac{\dot{T}_w}{\sigma^2 T_w}\theta + \frac{\dot{\sigma}}{\sigma^3}\eta\theta' + \frac{A}{\sigma^2}\left(nf'\theta - f\theta'\right) = \frac{1}{\mathrm{Pr}}(1+Nr)\theta'', \\ & \theta'(\eta=0) = -Bi(1-\theta(0)), \quad \theta(\eta\to\infty) = 0. \end{aligned} \tag{30}$$

Where $\Pr = \frac{\mu Cp}{\kappa}$ is the usual Prandtl number, $Nr = \frac{16\sigma^* T_\infty^3}{3k^*\kappa_f}$ is radiation term. The initial temperature condition in Eq. (5) and (6(e))–(6(g)) is imposed as

$$T_0(x, y) = T_\infty + T_a T_w(0)\left(\frac{x}{l}\right)^n \theta(\eta)\Big|_{\tau=0}.$$

Model 1 *Considering the flow model Eqs. (19) and (20), we may rewrite Eq. (30) as*

$$\begin{aligned} &\frac{\dot{T}_w}{AT_w}\theta + \frac{\alpha}{2}\eta\theta' + nf'\theta - f\theta' = \frac{1}{\Pr}(1+Nr)\theta'', \\ &\theta'(\eta=0) = -Bi\,(1-\theta(0)), \quad \theta(\eta\to\infty) = 0. \end{aligned} \tag{31}$$

We may deduce from Eq. (31) that separable temperature solutions exist only when $T_w = A^\beta$, with $\beta \geq 0$ so that Eq. (31) is now

$$\begin{aligned} &\alpha\left(\beta\theta + \frac{\eta}{2}\theta'\right) + nf'\theta - f\theta' = \frac{1}{\Pr}(1+Nr)\theta'', \\ &\theta'(\eta=0) = -Bi\,(1-\theta(0)), \quad \theta(\eta\to\infty) = 0. \end{aligned} \tag{32}$$

Exact solution for Eq. (32), took new variable $t = e^{-\lambda\eta}$ and $n = 2$, using this in Eq. (32) we get.

$$tZ_1\theta''(t) + (1 - M + Nt)\theta'(t) + L\theta(t) = 0, \tag{32a}$$

here

$$M = -\left(\frac{S}{\lambda} + \frac{d}{\lambda^2} - \frac{Z_2}{\lambda}\right), \qquad N = \frac{d}{\lambda^2 Z_1}, \quad L = \frac{2d}{\lambda^2} - \frac{Z_3}{\lambda^2 t},$$

to solve Eq. (32a) we use power series solution $\theta(t) = \sum_{r=0}^{\infty} a_r t^{r+k}$ by applying the Frobenius approach to get the unique behaviour and analytical solution obtained as

$$\begin{aligned} \theta'(0) = &\frac{\frac{Bi}{A_4}\left(e^{(-\lambda\eta)}\right)^{\frac{k_1+k_2}{2}} H\left[\frac{k_1+k_2}{2}, k_2+1, -Npe^{(-\lambda\eta)}\right]}{\left(\lambda\frac{k_1+k_2}{2}\right) H\left[\frac{k_1+k_2}{2}, k_2+1, -Np\right]}, \\ &- \frac{Np}{k_2+1} H\left[\frac{k_1+k_2}{2}+1, k_2+2, -Np\right] \\ &+ \frac{L}{A_4} H\left[\frac{k_1+k_2}{2}, k_2+1, -Np\right] \end{aligned} \tag{32b}$$

here

$$k_1 = M, \qquad k_2 = \sqrt{M^2 - 4L}, \qquad Z_1 = \frac{1}{\Pr}(1+Nr), \qquad Z_2 = \frac{2\alpha}{2}, \qquad Z_3 = \alpha\beta.$$

Notice that for a completely uniform wall temperature take (32), i.e., $n = \beta = 0$, the correct model is

$$\begin{aligned} &(1+Nr)\theta'' + \Pr f\theta' - \frac{\alpha}{2}\Pr\eta\theta' = 0, \\ &\theta'(\eta=0) = -Bi\,(1-\theta(0)), \quad \theta(\eta\to\infty) = 0. \end{aligned} \tag{33}$$

Which may be solved exactly in terms of improper integrals, but the numerical integration is preferred in what follows. In addition to this, majority of the literature dealt only with the wall heating case $\beta = 0$, *see, for instance,* (*Roşca and Pop* 2015; *Khalili et al.* 2015; *Nandy* 2015).

Theorem 3 *The unsteady system Eqs.* (2)–(6(*d*)) *under the constraints* (19) *and* (20) *has temperature field Eq.* (5) *and* (6(*e*))–(6(*g*)) *possessing separable temperature solutions Eq.* (29) *obtained from Eq.* (32), *with the wall temperature expressed by*

$T_w(\tau) = A(\tau)^\beta$, $\beta \geq 0$ *fixed, and* $n = 2$, *the resulting separable temperature field is given by*

$$T(x, y, \tau) = T_\infty + T_a A(\tau)^\beta \left(\frac{x}{l}\right)^2 \theta(\eta). \tag{34}$$

Proof Following closely the previous steps from Eqs. (31)–(34) will end up with the proof. □

Model 2 *Taking into account the model Eqs.* (22)–(26) *and* (27), *we may rewrite Eq.* (30) *as*

$$\begin{aligned} &\frac{\dot{T}_w}{T_w}\theta + A\left(2f'\theta - f\theta'\right) = \frac{1}{\mathrm{Pr}}(1 + Nr)\theta'', \\ &\theta'(\eta = 0) = -Bi(1 - \theta(0)), \quad \theta(\eta \to \infty) = 0. \end{aligned} \tag{35}$$

System Eq. (35) *suggests that the similarity solution form is not possible in general. However, keeping Eq.* (24) *in mind, we may only accomplish the similarity form when*

$$T_w(t) = A(t), \quad \mathrm{Pr} = 1, \theta = e^{-\lambda\eta}. \tag{36}$$

Otherwise, non-similar temperature solutions should be sought.

Theorem 4 *The system Eqs.* (2) *to* (6(*d*)) *under the constraints Eqs.* (22)–(26) *has no temperature field Eq.* (29) *possessing the separable temperature solutions of the form Eq.* (29), *and* $n = 2$, *unless* $\mathrm{Pr} = 1$ *and* $T_w(t) = A(t)$, *with the corresponding separable temperature field*

$$T(x, y, t) = T_\infty + T_a A(at)\left(\frac{x}{l}\right)^2 e^{-\lambda\sqrt{\frac{a}{\nu}}y}, \tag{37}$$

where $A(t)$ *is given by Eq.* (26).

Proof The proof is completed by following closely the previous steps from Eqs. (35) to (36). □

Corollary 2 *On account of the form of the solutions in Eqs.* (34) *and* (37), *the Nusselt number of engineering interest in Models* 1 *and* 2 *is given, respectively, via*

$$\begin{aligned} \left.\frac{\partial T}{\partial y}\right|_{y=0} &= T_a A(\tau)^\beta \sqrt{\frac{a}{\nu}} \frac{1}{\sqrt{1 - a\alpha t}} \left(\frac{x}{l}\right)^2 \theta'(0), \\ \left.\frac{\partial T}{\partial y}\right|_{y=0} &= -T_a A(at)\left(\frac{x}{l}\right)^2 \lambda\sqrt{\frac{a}{\nu}}. \end{aligned} \tag{38}$$

Table 1 Comparison table of skin friction at $S = 2.1$, $\Lambda \to \infty$, $Nr = 0$, $Bi = 0$, for stretching and shrinking surface in Model 1

	$\alpha = -0.5$ (Turkyilmazoglu 2024)	Present work	$\alpha = -1$ (Turkyilmazoglu 2024)	Present work	$\alpha = -1.5$ (Turkyilmazoglu 2024)	Present work
$d = 1$	2.40723	2.38899	2.31444	2.29115	2.22162	2.12113
$d = -1$	−1.09329	−1.08119	−0.78492	−0.68492	−0.40299	−0.39999

Table 2 Comparison table of heat transfer rate at $S = 2.1$, $\alpha = -1$, $\Lambda \to \infty$, $Nr = 0$, $Bi = 0$, $n = 0$ for stretching and shrinking surface in Model 1

	$\beta = 0$ (Turkyilmazoglu 2024)	Present work	$\beta = 0.5$ (Turkyilmazoglu 2024)	Present work	$\beta = 1$ (Turkyilmazoglu 2024)	Present work
$d = 1$	2.48103	2.48112	2.30486	2.29215	2.10506	2.10003
$d = -1$	2.01651	2.00231	1.74395	1.68592	1.36831	1.22162

3.1 Numerical procedure

Considered new terms to formulate greater order to a ordinary differential Eqs. (20) and (32).

$$y_1 = f, y_2 = f', y_3 = f'', y_4 = \theta, y_5 = \theta'. \tag{39}$$

The considered Eqs. (20)–(32) are formulated to first-order ODE as

$$\begin{aligned} y_2^1 &= y_3, y_3^1 = -\left(\left(1/\left(1+\Lambda^{-1}\right)\right)\left(y_1 y_3 - y_2^2 - \alpha y_2 - \alpha \frac{\eta}{2} y_3\right)\right), \\ y_4^1 &= y_5, y_5^1 = -\left(\left(\frac{\Pr}{(1+Nr)}\right)\left(\alpha\beta y_4 + \frac{\alpha\eta}{2} y_5 + n y_2 y_4 - y_1 y_5\right)\right), \end{aligned} \tag{40}$$

3.2 Analytical procedure

- Governing Eqs. (2) to (5) are solved by using the similarity variable sin Eq. (15).
- By solving the momentum Eq. (3), we obtained the ODE Eq. (18), after by using Eq. (19) we got the Eq. (20) and (20a) we obtained the analytical solutions binary roots in Eq. (20c).
- The temperature Eq. (29) used to solve the Eq. (5) to get the Eq. (30), by utilising the Eq. (31) and (32) and applying the hypergeometric series solution method to solve the temperature ODE equation and got the analytical solution for the temperature (32b).

3.3 The validation and model verification

To verify the present model, we used the skin friction values in Table 1 and compare with data available by Turkyilmazoglu (2024). Then we compare heat transfer rates with the data in Table 2. It can be found that the current model agrees well with data by Turkyilmazoglu (2024). And also, Table 3 compared the numerical values with Hayat et al. (2011) and Ibrahim and Shankar (2013) found that the numerical values agree with the data and the present model was validated.

Table 3 Comparison table of local Nusselt number $-\theta'(0)$ at $\Lambda \to \infty$, $\alpha = 0$, $Nr = 0$, $Bi = 0$, $d = 1$. For various values of Prandtl number and mass transpiration S with earlier published data when power of $\left(\frac{x}{l}\right)$ is one

S	Pr	Hayat et al. (2011)	Ibrahim and Shankar (2013)	Present results
−1.5	0.72	0.4570273	0.4570	0.4570002
	1	0.5000000	0.5000	0.5000000
	10	0.6451648	0.6442	0.6451601
0	0.72	0.8086314	0.8086	0.8086334
	1	1.0000000	1.0000	1.0000000
	3	1.9235913	1.9237	1.9235913
	10	3.7215968	3.7107	3.7159601
1.5	0.72	1.4943687	1.4944	1.4943688
	1	2.0000621	2.0000	2.0000000
	10	16.096248	16.0842	16.096249

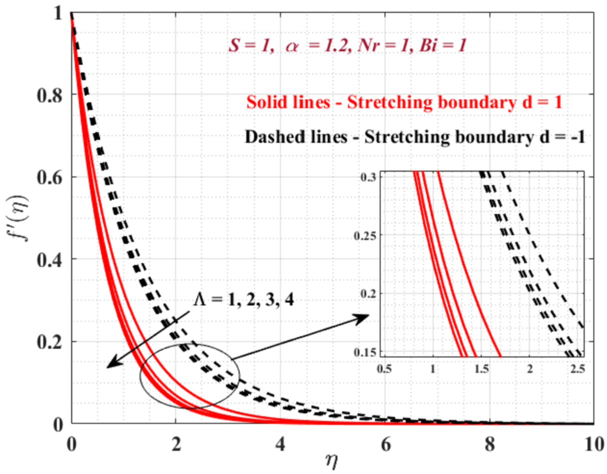

Fig. 2 Casson parameter effect on velocity

4 Results and discussion

This analysis gives insight into unsteady radiative energy and Casson fluid flow across stretching and shrinking sheets with Biot boundary conditions, enhancing our comprehension of these intricate conditions. We examined two mathematical representations using a rigorous method. The initial model aligns with the model usually used by scientists in this area, but its stationary solution stays trivial. The second model, presented in this analysis, clearly illustrates the physically pertinent stationary solutions well examined in published works. Analysed both analytical and numerical methods and studied many physical effects as follows:

Figure 2 represents the momentum graph for different choices of Casson term, here solid lines portray the stretching boundary and dashed lines portrays the shrinking boundary case. Enhancing the Casson term decreases the axial momentum of the fluid movement. Physically, The Casson parameter greatly affects the velocity of fluid flow in non-Newtonian

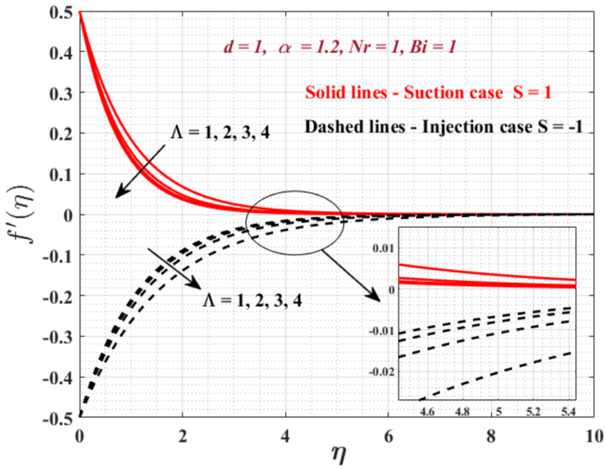

Fig. 3 Casson parameter influence on velocity for suction/injection

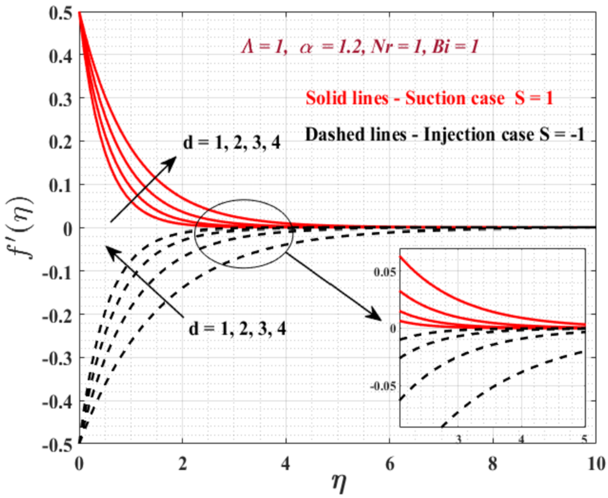

Fig. 4 Stretching parameter influence on velocity

fluids. An upsurge in the Casson term typically causes the velocity to decrease due to the increased plastic dynamic viscosity, which introduces opposition to flow.

Figure 3 represents the momentum graph for different choices of Casson term, here solid lines portray the suction and dashed lines represents the injection case. Upsurging the Casson term slow downs the axial momentum of the fluid flow. For suction case the solution obtained in the positive region while in injection case solution delves in negative region. Physically, the Casson term significantly impacts on the velocity of fluid flow in non-Newtonian fluids. An upsurge in the Casson term typically causes the velocity to decrease profile due to the increased plastic dynamic viscosity, which introduces resistance to flow.

Figure 4 represents the velocity graph for various choices of stretching term, here solid lines portray the suction and dashed lines represents the injection case. Enhancing the stretching parameter upsurges the velocity of the fluid movement. For suction case the solution obtained in the positive region while in injection case solution delves in negative region. Physically, the stretching parameter significantly influences axial velocity in fluid dynamics. Enhancing the stretching parameter enhances the velocity of nanofluids due to reduced

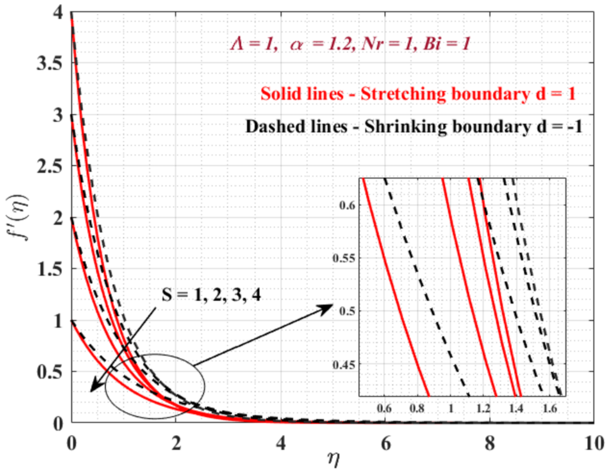

Fig. 5 Suction parameter influence on velocity

viscous effects, leading to a thinner momentum boundary layer. Conversely, for shrinking surfaces, higher stretching parameters result in decreased velocity due to increased resistance from viscosity.

Figure 5 represents the velocity graph for various choices of suction term; here solid lines portray the stretching and dashed lines represent the shrinking case. Upsurging the suction parameter reduces the axial velocity. Physically, mass transpiration significantly affects fluid flow velocity. Increasing suction decreases the fluid velocity as it pulls the fluid towards the boundary, enhancing viscosity and decelerating flow. Conversely, injection of fluid accelerates the flow, pushing heated fluid far from the boundary and reducing viscous effects, resulting in higher velocities.

Figure 6(a) represents the temperature graph for different values of Biot number term for suction/injection case, and here solid lines portray the suction and dashed lines represents the injection case, and 6(b) for stretching/shrinking boundary, solid lines represent the stretching and dashed lines represent the shrinking case, Upsurging the Biot number parameter decays the temperature of the liquid flow. Physically, the Biot number is a dimensionless quantity that influences energy distribution in heat transfer scenarios. It represents the ratio of heat resistance due to conduction within a body to that due to convection at its surface. Low Biot numbers indicate uniform temperature within the body, simplifying analysis via lumped capacitance models. High Biot numbers suggest significant internal temperature gradients, necessitating more complex analysis methods.

Figure 7(a) represents the temperature graph for different choices of radiation terms, here solid lines portray the stretching and dashed lines represent the shrinking case and 7(a) solid lines portray the suction and dashed lines portrays the injection case. Upsurges the thermal radiation term increases the temperature of the liquids flow. Physically, the thermal radiation significantly impacts the temperature of fluid flow by enhancing heat transfer rates and fluid properties. As the radiation term enhances, the energy of the fluid typically rises due to enhanced heat absorption. However, this impact can be counterbalanced by factors such as the Prandtl number; greater Prandtl numbers often lead to reduced temperatures due to decreased thermal conductivity.

Figure 8(a-d) represent the streamline graphs for various numbers of Casson term for both suction and injection cases, streamline graphs for different Casson parameters provide insight into how fluid motion is influenced under varying physical conditions. In both suction

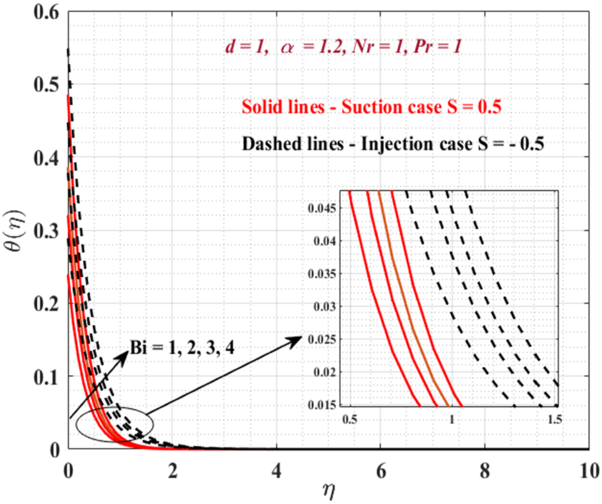

(a)

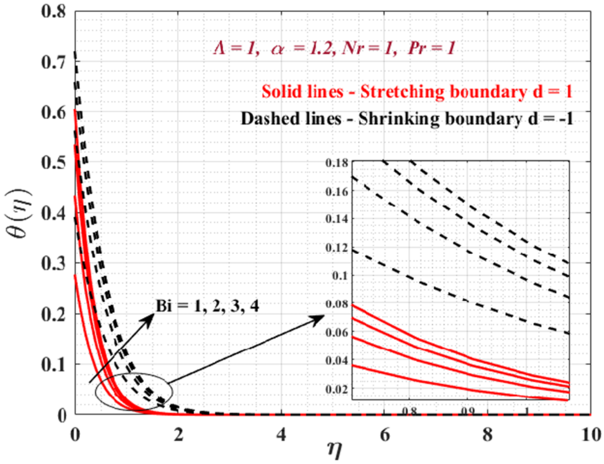

(b)

Fig. 6 (a): Biot parameter effect on energy profile for suction/injection case. (b): Biot parameter effect on energy profile

and injection cases, they help visualize boundary layer behavior, flow separation, and mixing characteristics. Such analysis is important for optimizing engineering systems involving heat transfer, drag reduction, and fluid control.

4.1 Summary of model behavior and conceptual contribution

The present analysis reveals two distinct unsteady formulations. Model 1, which resembles the commonly used equations in previous studies, evolves only into a trivial steady state, demonstrating that earlier unsteady formulations cannot recover the classical Sakiadis-Crane or Miklavčič-Wang solutions. Nevertheless, Model 1 admits separable similarity solutions for both velocity and temperature fields, including new similarity variables for the energy

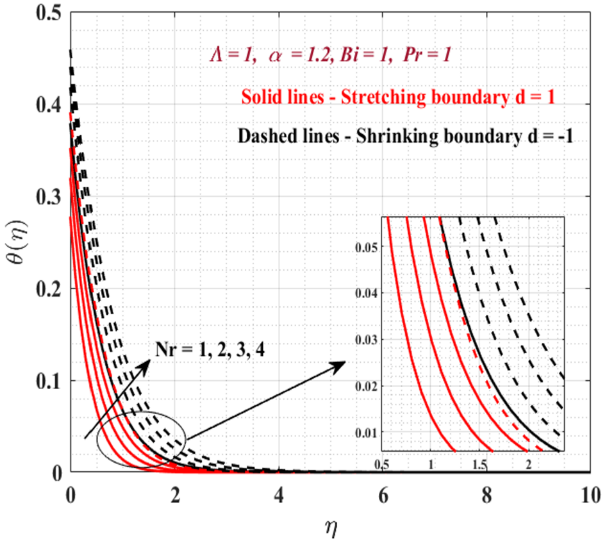

(a)

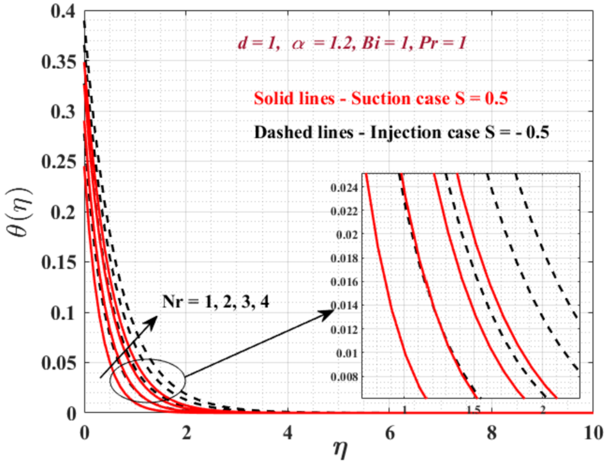

(b)

Fig. 7 (a): Radiation parameter effect temperature. (b): Radiation term influence temperature for suction/injection case

equation that have not been reported in the literature. In contrast, Model 2 satisfies the correct far-field conditions required for physically meaningful unsteady-to-steady evolution and successfully converges to the established non-trivial steady states. Although Model 2 does not generally yield a similarity temperature solution, it preserves the correct physical behavior of the boundary layer. The main conceptual contribution of this study lies in identifying and resolving the longstanding inconsistency in unsteady modeling: we show mathematically that traditional unsteady formulations cannot approach the correct steady-state limits, whereas our new formulation does. This provides a more consistent theoretical framework for future unsteady analyses over stretching and shrinking surfaces.

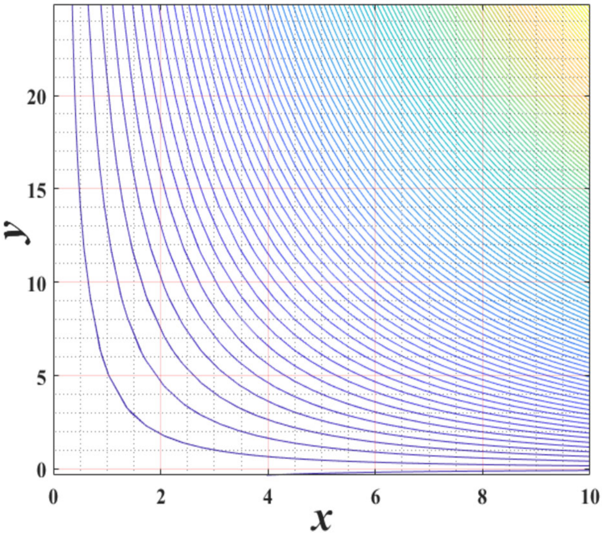

(a)

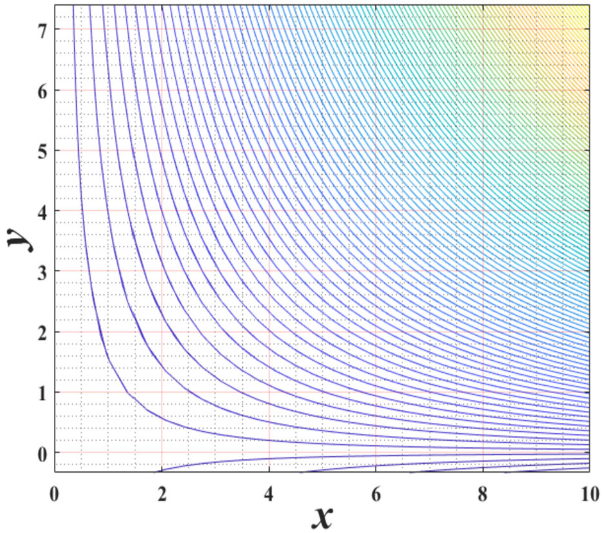

(b)

Fig. 8 (a): Stream lines for mass injection at $\Lambda = 0.1$. (b): Stream lines for mass suction at $\Lambda = 0.1$. (c): Stream lines for mass injection at $\Lambda = 3$. (d): Stream lines for mass suction at $\Lambda = 3$

5 Concluding remarks

Since the available studies in unsteady heat and fluid flow equations associated with the plane stretching/shrinking sheets that do not converge to the steady state results of the Sakiadis (1961), Crane (1970) and Miklavčič and Wang (2006). Therefore, this paper aims to address this issue through the unsteady state mathematical description of the Navier-Stokes equations. The analysis demonstrates further that, mathematically, it is possible to arrive at

Fig. 8 (*Continued*)

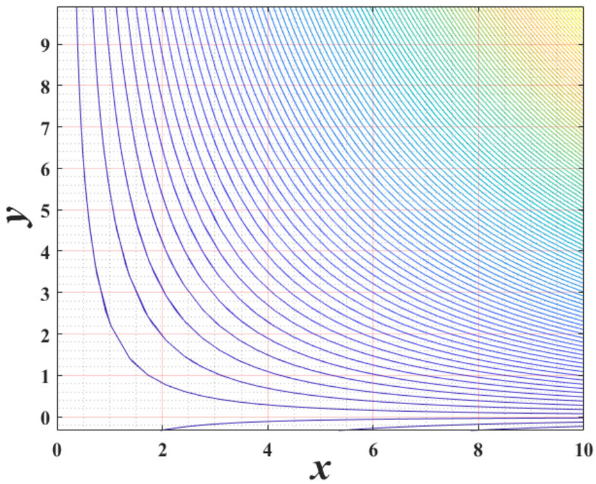

(c)

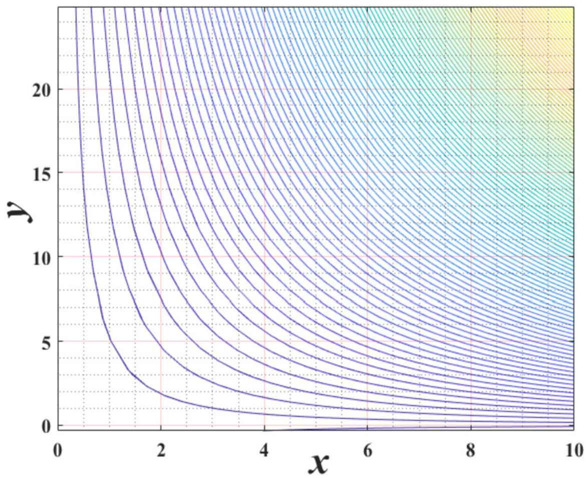

(d)

two distinctly different unsteady flow models. The existence of these models has been shown in the corresponding flow and heat theorems. The first model which this work has attempted to conceptualize widely, is most preferred by active researchers. Unfortunately, this one has the trivial steady-state solution. Moreover, this model permits the introduction of new similarity equations in the temperature field, which have not been reported previously. From the temperature field distribution plots, the optimum heat transfer implies that the wall should be kept at a uniform temperature. This is one of the findings that it is important for investigators in the field to note. The second unsteady flow model, on the other hand, is completely in agreement with the well-known steady-state solutions of Sakiadis (1961), Crane (1970) and Miklavčič and Wang (2006). Findings of the current study reveal as follows:

- Enhancing the Casson parameter decays the velocity for both expanding and shrinking boundaries.
- Upsurging the stretching term increases the velocity profile.

- Increasing the thermal radiation enhances the temperature profile.
- Upsurging the Biot number improves the temperature profile.
- Enhancing the mass suction slowdowns the velocity boundary layer.

The future scope of the current study lies in its potential to advance understanding in energy distribution and fluid dynamics. The results could contribute to more efficient thermal management in industrial uses, like energy systems and material processing. Additionally, the novel time-dependent solutions could be further refined to address complex real-world scenarios involving non-Newtonian fluids. Further exploration into varying boundary conditions and more diverse fluid models could expand the study's practical relevance in engineering and environmental sciences.

Acknowledgements L. M. Pérez gratefully acknowledges financial support from the Centers of Excellence with BASAL/ANID CIA250002, CEDENNA. Mr. Sachhin S. M. sincerely thanks the University of Tarapacá (Chile), for the kind invitation and generous hospitality extended to him as a visiting scholar through the Visiting Researchers Program during the academic year 2025-2026. He expresses his deep gratitude to his research supervisor, Professor U. S. Mahabaleshwar, for his constant guidance and support, and also extends sincere thanks to Prof. L. M. Pérez (Universidad de Tarapacá), for her warm hospitality and valuable assistance during his visit.

Funding information No funding.

Data availability The datasets used and/or analyzed during the current study available from the corresponding author on reasonable request.

Declarations

Competing interests The authors declare no competing interests.

References

Aljedani, J., et al.: Magnetohydrodynamic and convective heating analysis of chemically active iron oxide and gold nanoparticles based hybrid blood flow over a radiated sheet. BioNanoScience **15**(1), 50 (2024). https://doi.org/10.1007/s12668-024-01680-x

Amanulla, C.H., Nagendra, N., Subba Rao, A., Anwar Bég, O., Kadir, A.: Numerical exploration of thermal radiation and Biot number effects on the flow of a non-Newtonian MHD Williamson fluid over a vertical convective surface. Heat Transf. Asian Res. **47**(2), 286–304 (2018). https://doi.org/10.1002/htj.21303

Animasaun, I.L., Adebile, E.A., Fagbade, A.I.: Casson fluid flow with variable thermo-physical property along exponentially stretching sheet with suction and exponentially decaying internal heat generation using the homotopy analysis method. J. Niger. Math. Soc. **35**(1), 1–17 (2016). https://doi.org/10.1016/j.jnnms.2015.02.001

Arthur, E.M., Seini, I.Y., Bortteir, L.B.: Analysis of Casson Fluid Flow over a Vertical Porous Surface with Chemical Reaction in the Presence of Magnetic Field. J. Appl. Math. Phys. **3**(6) (2015). https://doi.org/10.4236/jamp.2015.36085

Awais, M., Khalil-Ur-Rehman, Malik, M.Y., Hussain, A., Salahuddin, T.: A computational analysis subject to thermophysical aspects of Sisko fluid flow over a cylindrical surface. Eur. Phys. J. Plus **132**(9), 392 (2017). https://doi.org/10.1140/epjp/i2017-11645-y

Basir, M.F.M., et al.: Stability analysis of unsteady stagnation-point gyrotactic bioconvection flow and heat transfer towards the moving sheet in a nanofluid. Chin. J. Phys. **65**, 538–553 (2020). https://doi.org/10.1016/j.cjph.2020.02.021

Bataller, R.C.: Viscoelastic fluid flow and heat transfer over a stretching sheet under the effects of a non-uniform heat source, viscous dissipation and thermal radiation. Int. J. Heat Mass Transf. **50**(15), 3152–3162 (2007). https://doi.org/10.1016/j.ijheatmasstransfer.2007.01.003

Bég, O.A., Uddin, M.J., Rashidi, M.M., Kavyani, N.: Double-diffusive radiative magnetic mixed convective slip flow with Biot and Richardson number effects. J. Eng. Thermophys. **23**(2), 79–97 (2014). https://doi.org/10.1134/S1810232814020015

Crane, L.J.: Flow past a stretching plate. Z. Angew. Math. Phys. **21**(4), 645–647 (1970). https://doi.org/10.1007/BF01587695

Darvesh, A., et al.: Thermal diffusivity of inclined magnetized Cross fluid with temperature dependent thermal conductivity: spectral relaxation scheme. Discov. Appl. Sci. **6**(3), 117 (2024a). https://doi.org/10.1007/s42452-024-05691-x

Darvesh, A., Santisteban, L.J.C., Khan, S., Maiz, F.M., Garalleh, H.A.L., Sánchez-Chero, M.: Numerical simulation of melting heat transport mechanism of Cross nanofluid with multiple features of infinite shear rate over a Falkner-Skan wedge surface. J. Appl. Math. Mech. **104**(11), e202400218 (2024b). https://doi.org/10.1002/zamm.202400218

Darvesh, A., et al.: Radiative heat transfer in MHD copper-based polymer nanofluid over a sphere using larger radius and inter particle spacing of nanoparticles. Results Eng. **26**, 105012 (2025). https://doi.org/10.1016/j.rineng.2025.105012

Deepalakshmi, P., Darvesh, A., Garalleh, H.A., Sánchez-Chero, M., Shankar, G., Siva, E.P.: Integrate mathematical modeling for heat dynamics in two-phase Casson fluid flow through renal tubes with variable wall properties. Ain Shams Eng. J. **16**(1), 103183 (2025). https://doi.org/10.1016/j.asej.2024.103183

Dharmaiah, G., Goud, B.S., Srinivasulu, T., Sridevi, M., Srinu, A.: Influence of activation energy in steady state hydro dynamic non-Newtonian nano fluid with mobile microorganisms. Results Chem. **9**, 101653 (2024). https://doi.org/10.1016/j.rechem.2024.101653

Farooq, U., Razzaq, R., Khan, M.I., Chu, Y.-M., Lu, D.C.: Modeling and numerical computation of nonsimilar forced convective flow of viscous material towards an exponential surface. Int. J. Mod. Phys. B **35**(08), 2150118 (2021). https://doi.org/10.1142/S0217979221501186

Gaffar, S.A., Prasad, V.R., Bég, O.A.: Numerical study of flow and heat transfer of non-Newtonian tangent hyperbolic fluid from a sphere with Biot number effects. Alex. Eng. J. **54**(4), 829–841 (2015). https://doi.org/10.1016/j.aej.2015.07.001

Gosty, V., Srinivas, G., Babu, B.S., Goud, B.S., Hendy, A.S., Ali, M.R.: Influence of variable viscosity and slip on heat and mass transfer of immiscible fluids in a vertical channel. Case Stud. Therm. Eng. **58**, 104368 (2024). https://doi.org/10.1016/j.csite.2024.104368

Goud, B.S., Reddy, Y.D., Duraihem, F.Z.: Numerical approach of NiZnFe2O4 (nickel–zinc ferrite) — ethylene glycol magneto nanofluid flow over a porous shrinking sheet with chemical reaction and radiation. NANO **19**(12), 2450071 (2024). https://doi.org/10.1142/S1793292024500711

Hamid, A., Hashim, Hafeez, A., Khan, M., Alshomrani, A.S., Alghamdi, M.: Heat transport features of magnetic water–graphene oxide nanofluid flow with thermal radiation: stability test. Eur. J. Mech. B, Fluids **76**, 434–441 (2019). https://doi.org/10.1016/j.euromechflu.2019.04.008

Hashim, Hamid, A., Khan, M., Khan, U.: Thermal radiation effects on Williamson fluid flow due to an expanding/contracting cylinder with nanomaterials: dual solutions. Phys. Lett. A **382**(30), 1982–1991 (2018a). https://doi.org/10.1016/j.physleta.2018.04.057

Hashim, Khan, M., Sharjeel, Khan, U.: Stability analysis in the transient flow of Carreau fluid with non-linear radiative heat transfer and nanomaterials: critical points. J. Mol. Liq. **272**, 787–800 (2018b). https://doi.org/10.1016/j.molliq.2018.08.049

Hashim, Khan, M., Hamid, A.: Convective heat transfer during the flow of Williamson nanofluid with thermal radiation and magnetic effects. Eur. Phys. J. Plus **134**(2), 50 (2019). https://doi.org/10.1140/epjp/i2019-12473-9

Hayat, T., Qasim, M., Mesloub, S.: MHD flow and heat transfer over permeable stretching sheet with slip conditions. Int. J. Numer. Methods Fluids **66**(8), 963–975 (2011). https://doi.org/10.1002/fld.2294

Hussain, A., Malik, M.Y.: MHD nanofluid flow over stretching cylinder with convective boundary conditions and Nield conditions in the presence of gyrotactic swimming microorganism: a biomathematical model. Int. Commun. Heat Mass Transf. **126**, 105425 (2021). https://doi.org/10.1016/j.icheatmasstransfer.2021.105425

Hussain, M., Khan, W., Farooq, U., Razzaq, R.: Impact of non-similar modeling for thermal transport analysis of mixed convective flows of nanofluids over vertically permeable surface. J. Nanofluids **12**(4), 1074–1081 (2023). https://doi.org/10.1166/jon.2023.1985

Hussain, A., Ayub, S., Salahuddin, T., Khan, M., Altanji, M.: Numerical study of binary mixture and thermophoretic analysis near a solar radiative heat transfer. Chaos Solitons Fractals **183**, 114962 (2024a). https://doi.org/10.1016/j.chaos.2024.114962

Hussain, A., Kazmi, S.N., Bilal, S.: Induction of platelet-shaped ferromagnetic nanoparticles to analyze heat transport mechanism in peristaltic activity of blood-based Casson liquid in non-symmetric configuration with heat source and viscous dissipation aspects. J. Therm. Anal. Calorim. **149**(22), 13031–13043 (2024b). https://doi.org/10.1007/s10973-024-13681-9

Ibrahim, W., Shankar, B.: MHD boundary layer flow and heat transfer of a nanofluid past a permeable stretching sheet with velocity, thermal and solutal slip boundary conditions. Comput. Fluids **75**, 1–10 (2013). https://doi.org/10.1016/j.compfluid.2013.01.014

Kazmi, S.N., Hussain, A., Rehman, K.U., Shatanawi, W.: Thermal analysis of hybrid nanoliquid contains iron-oxide (Fe3O4) and copper (Cu) nanoparticles in an enclosure. Alex. Eng. J. **101**, 176–185 (2024). https://doi.org/10.1016/j.aej.2024.05.098

Khalili, S., Tamim, H., Khalili, A., Rashidi, M.M.: Unsteady convective heat and mass transfer in pseudoplastic nanofluid over a stretching wall. Adv. Powder Technol. **26**(5), 1319–1326 (2015). https://doi.org/10.1016/j.apt.2015.07.006

Kumar, V.V., Shekar, M.N.R., Bejawada, S.G.: Thermo-diffusion, diffusion-thermo impacts on heat and mass transfer Casson fluid flow with porous medium in the presence of heat generation and radiation. Partial Differ. Equ. Appl. Math. **13**, 101039 (2025). https://doi.org/10.1016/j.padiff.2024.101039

Liu, X., Zhang, C., Song, L., Li, J.: Influence of Biot number and geometric parameters on the overall cooling effectiveness of double wall structure with pins. Appl. Therm. Eng. **198**, 117439 (2021). https://doi.org/10.1016/j.applthermaleng.2021.117439

Mahabaleshwar, U.S., Sachhin, S.M., Pérez, L.M., Lorenzini, G.: An effect of mass transpiration and Darcy-Brinkman model on Ostwald-de Waele ternary nanofluid. J. Eng. Thermophys. **33**(3), 547–565 (2024). https://doi.org/10.1134/S181023282403010X

Miklavčič, M., Wang, C.: Viscous flow due to a shrinking sheet. Q. Appl. Math. **64**(2), 283–290 (2006). https://doi.org/10.1090/S0033-569X-06-01002-5

Mittal, A.S., Patel, H.R.: Influence of thermophoresis and Brownian motion on mixed convection two dimensional MHD Casson fluid flow with non-linear radiation and heat generation. Phys. Stat. Mech. Appl. **537**, 122710 (2020). https://doi.org/10.1016/j.physa.2019.122710

Mohamad Isa, S., et al.: Thermal radiative and Hall current effects on magneto-natural convective flow of dusty fluid: numerical Runge–Kutta–Fehlberg technique. Numer. Heat Transf., Part B, Fundam. **86**, 1599–1621 (2025). https://doi.org/10.1080/10407790.2024.2318452

Nandy, S.K.: Unsteady flow of Maxwell fluid in the presence of nanoparticles toward a permeable shrinking surface with Navier slip. J. Taiwan Inst. Chem. Eng. **52**, 22–30 (2015). https://doi.org/10.1016/j.jtice.2015.01.025

Prasad, V.R., Gaffar, S.A., Reddy, E.K., Bég, O.A.: Computational Study of Non-Newtonian Thermal Convection from a Vertical Porous Plate in a Non-Darcy Porous Medium with Biot Number Effects. J. Porous Media **17**(7) (2014). https://doi.org/10.1615/JPorMedia.v17.I7.40

Razzaq, R., Farooq, U.: Non-similar analysis of MHD hybrid nanofluid flow over an exponentially stretching/shrinking sheet with the influences of thermal radiation and viscous dissipation. Numer. Heat Transf., Part B, Fundam. **86**(5), 1398–1413 (2025). https://doi.org/10.1080/10407790.2024.2312958

Razzaq, R., Farooq, U., Mirza, H.R.: Nonsimilar forced convection analysis of Maxwell nanofluid flow over an exponentially stretching sheet with convective boundary conditions. J. Appl. Math. Mech. **103**(12), e202200623 (2023). https://doi.org/10.1002/zamm.202200623

Razzaq, R., Sagheer, S., Farooq, U.: Local non-similar solutions of magnetohydrodynamic Casson nanofluid flow over a non-linear inclined surface with thermal radiation and heat generation effects: a utilization of up to third truncation. J. Porous Media **27**(6) (2024). https://doi.org/10.1615/JPorMedia.2023049654

Roşca, N.C., Pop, I.: Unsteady boundary layer flow over a permeable curved stretching/shrinking surface. Eur. J. Mech. B, Fluids **51**, 61–67 (2015). https://doi.org/10.1016/j.euromechflu.2015.01.001

Sachhin, S.M., Mahabaleshwar, U.S.: Bioconvection impact on chemically reactive Prandtl–Eyring nanofluid flow through Darcy–Forchheimer media based on Buongiorno's framework. Phys. Fluids **37**(6), 063124 (2025). https://doi.org/10.1063/5.0276888

Sachhin, S.M., Granados-Ortiz, F.-J., Mahabaleshwar, U.S., Ortega-Casanova, J., Pérez, L.M.: Heat and mass transfer analysis of a Bingham ternary nanofluid exposed to radiation over stretching/shrinking sheets and Stefan blowing effect. Alex. Eng. J. **129**, 515–529 (2025a). https://doi.org/10.1016/j.aej.2025.06.026

Sachhin, S.M., Mahabaleshwar, U.S., Nayakar, S.N.R., Patil, H.S.R., Souayeh, B.: Darcy–Brinkman model for Boussinesq–Stokes suspension tetra dusty nanofluid flow over stretching/shrinking sheet with suction/injection. Numer. Heat Transf., Part A, Appl. **86**, 8288–8310 (2025b). https://doi.org/10.1080/10407782.2024.2359047

Sachhin, S.M., Mahabaleshwar, U.S., Swaminathan, N., Laroze, D., Pedraja-Rejas, L.: An effect of waste discharge concentration and electromagnetic field on chemically reactive Bingham fluid flow with the analysis entropy generation and mass transfer. Hyb. Adv. **8**, 100344 (2025c). https://doi.org/10.1016/j.hybadv.2024.100344

Sachhin, S.M., Mahabaleshwar, U.S., Swaminathan, N., Pérez, L.M., Wang, J.: Thermal dynamics and magnetohydrodynamics in ferrofluidic wall jet flow: entropy generation in heat and mass transfer. J. Mol. Liq. **427**, 127449 (2025d). https://doi.org/10.1016/j.molliq.2025.127449

Sagheer, S., Razzaq, R., Vafai, K.: Local non-similar solutions for EMHD nanofluid flow with radiation and variable heat flux along a stretching sheet. Numer. Heat Transf., Part A, Appl. **85**(22), 3923–3940 (2024). https://doi.org/10.1080/10407782.2024.2360082

Saif, R.S., Hashim, Zaman, M., Ayaz, M.: Thermally stratified flow of hybrid nanofluids with radiative heat transport and slip mechanism: multiple solutions. Commun. Theor. Phys. **74**(1), 015801 (2021). https://doi.org/10.1088/1572-9494/ac3230

Sakiadis, B.C.: Boundary-layer behavior on continuous solid surfaces: I. Boundary-layer equations for two-dimensional and axisymmetric flow. AIChE J. **7**(1), 26–28 (1961). https://doi.org/10.1002/aic.690070108

Shah, I.A., Bilal, S., Asjad, M.I., Tag-ElDin, E.M.: Convective Heat and Mass Transport in Casson Fluid Flow in Curved Corrugated Cavity with Inclined Magnetic Field. Micromachines **13**(10) (2022). https://doi.org/10.3390/mi13101624

Sheremet, M.A., Pop, I.: Natural convection combined with thermal radiation in a square cavity filled with a viscoelastic fluid. Int. J. Numer. Methods Heat Fluid Flow **28**(3), 624–640 (2018). https://doi.org/10.1108/HFF-02-2017-0059

Srinivas, G., Babu, B.S., Goud, B.S.: SLIP effects on heat and mass transfer through CuO-water nanofluid in a horizontal channel heated at center. J. Therm. Anal. Calorim. **149**(22), 13267–13283 (2024). https://doi.org/10.1007/s10973-024-13686-4

Turkyilmazoglu, M.: Two models on the unsteady heat and fluid flow induced by stretching or shrinking sheets and novel time-dependent solutions. ASME J. Heat Mass Transf. **146**, 101802 (2024). https://doi.org/10.1115/1.4065674

Yu, D., Wang, R.: An optimal investigation of convective fluid flow suspended by carbon nanotubes and thermal radiation impact. Mathematics **10**(9), 1524 (2022). https://doi.org/10.3390/math10091542

Authors and Affiliations

S.M. Sachhin[1] · M.S. Bharath[1] · U.S. Mahabaleshwar[1] · G.V. Bognar[2] · L.M. Pérez[3]

✉ U.S. Mahabaleshwar
u.s.m@davangereuniversity.ac.in

S.M. Sachhin
sachinsm030@gmail.com

M.S. Bharath
bharathms925@gmail.com

G.V. Bognar
v.bognar.gabriella@uni-miskolc.hu

L.M. Pérez
lperez@academicos.uta.cl

1 Department of Studies in Mathematics, Davangere University, Shivagangothri, Davangere, 577 007, India

2 Institute of Machine and Product Design, University of Miskolc, 3515 Miskolc-Egyetemváros, Hungary

3 Departamento de Ingeniería Industrial y de Sistemas, Universidad de Tarapacá, Casilla 7D, Arica, 1000000, Chile